Journal of Power Sources 196 (2011) 7039–7043

Contents lists available at ScienceDirect

Journal of Power Sources

journal homepage: www.elsevier.com/locate/jpowsour

Short communication

Development of high power lithium-ion batteries: Layer $Li[Ni_{0.4}Co_{0.2}Mn_{0.4}]O_2$ and spinel $Li[Li_{0.1}Al_{0.05}Mn_{1.85}]O_4$

Seung-Taek Myung[a,*], Ki-Soo Lee[b], Yang-Kook Sun[b], Hitoshi Yashiro[a]

[a] Department of Chemical Engineering, Iwate University, 4-3-5 Ueda, Morioka, Iwate 020-8551, Japan
[b] Department of Energy Engineering, Hanyang University, Seoul 133-791, South Korea

ARTICLE INFO

Article history:
Received 7 July 2010
Received in revised form 3 September 2010
Accepted 4 September 2010
Available online 15 September 2010

Keywords:
$Li[Ni_{0.4}Co_{0.2}Mn_{0.4}]O_2$
$Li[Li_{0.1}Al_{0.05}Mn_{1.85}]O_4$
Positive electrode
Lithium
Battery

ABSTRACT

Layer $Li[Ni_{0.4}Co_{0.2}Mn_{0.4}]O_2$ and lithium excess spinel $Li[Li_{0.1}Al_{0.05}Mn_{1.85}]O_4$ were compared as positive electrode materials for high power lithium-ion batteries. Physical properties were examined by Rietveld refinement of X-ray diffraction pattern and scanning electron microscopic studies. From continuous charge and discharge tests at higher currents and different temperature environments using 3Ah class lithium-ion batteries, it was found that both materials presented plausible battery performances such as rate capability, cyclability at 60 °C at elevated temperature, and low temperature properties as well.

1. Introduction

Recently, a speedy increase in crude oil price and global environmental concerns give rise to a significant attention to the development of large format lithium batteries that store electricity. In order to adopt those as power sources, reliable power, capacity and safety are considered to be the most important criteria that should be satisfied [1]. Nickel-rich $Li[Ni_{1-x}M_x]O_2$ ($x \leq 0.2$) compounds such as $Li[Ni_{0.8}Co_{0.15}Al_{0.05}]O_2$ and $Li[Ni_{0.8}Co_{0.1}Mn_{0.1}]O_2$ have been intensively investigated as positive electrode materials for large format lithium battery applications because of their relatively low cost and high reversible capacity, approximately 200 mAh g^{-1} [2,3]. However, they have shown poor thermal stability due to oxygen release from the highly delithiated $Li_{1-\delta}[Ni_{1-x}M_x]O_2$, which reacts with the organic electrolyte and thus leads to thermal runaway [4,5]. Moreover, the unstable Ni^{4+} in the delithiated $Li_{1-\delta}[Ni_{1-x}M_x]O_2$ easily reduces to inactive NiO, resulting in high solid–electrolyte interfacial impedance and poor cycle life of the cell [6,7]. From those concerns, layer $Li[(Ni_{0.5}Mn_{0.5})_{1-x}Co_x]O_2$ ($x = 0$–$1/3$) and spinel $LiMn_2O_4$ or their derivatives are recommended though the resulting capacity is smaller than that of nickel-rich $Li[Ni_{1-x}M_x]O_2$ ($x \leq 0.2$) because those materials present relatively stable thermal stability [8–10].

Layer $Li[(Ni_{0.5}Mn_{0.5})_{1-x}Co_x]O_2$ ($x = 0$–$1/3$) has interesting material chemistry; the average oxidation state of Ni, Co, and Mn is 2+, 3+, and 4+, respectively. So, electrochemical activity is mainly attributed to redox couples of $Ni^{2+/3+/4+}$ and $Co^{3+/4+}$ [11,12], when it is cycled between 2.5 V and 5.0 V versus Li. Although Mn^{4+} does not join electrochemical reaction, the two electron reaction of Ni compensates for the electrochemically inactive Mn^{4+} on the voltage range. Besides, the inactive Mn^{4+} supports significant structural stability during repetitive Li^+ de-/intercalation and thermal stability as well [13,14].

Spinel type $LiMn_2O_4$ has been considered to be one of the most promising cathode materials, if the disproportionated Mn dissolution ($2Mn^{3+} \rightarrow Mn^{2+} + Mn^{4+}$) is solved. To overcome capacity fading upon cycling, a lot of trials were made; the manganese site replacement by other elements, $LiMMn_{2-x}O_4$ (M = Li, Al, Co, Ni, Fe, Cr, Zn, etc.) to enhance structural stability [15–21]. The capacity fading was obviously suppressed as the amount of dopant increased causing decrease of delivered capacity comparing to undoped $LiMn_2O_4$. Komaba et al. [15] suggested that $Li_{1.1}Mn_{1.9}O_4$ significantly suppressed the Mn dissolution due to stabilizing of the host structure by substituting Li for Mn in $LiMn_2O_4$.

For those reasons, in this study, we employed the layer $Li[Ni_{0.4}Co_{0.2}Mn_{0.4}]O_2$ and the lithium excess $Li[Li_{0.1}Al_{0.05}Mn_{1.85}]O_4$ as the positive electrode materials. Laminate-type 3 Ah class lithium-ion cells were fabricated and the cell performances were compared as high power lithium-ion batteries.

* Corresponding author. Tel.: +81 19 321 6345; fax: +81 19 321 6345.
E-mail address: smyung@iwate-u.ac.jp (S.-T. Myung).

0378-7753/$ – see front matter © 2010 Elsevier B.V. All rights reserved.
doi:10.1016/j.jpowsour.2010.09.012

2. Experimental

$Li[Ni_{0.4}Co_{0.2}Mn_{0.4}]O_2$ and $Li[Li_{0.1}Al_{0.05}Mn_{1.85}]O_4$ powders synthetized via coprecipitation were employed as positive electrode materials. Detailed synthesis is reported elsewhere [22,10]. Powder X-ray diffraction (XRD, Rigaku, Rint-2200) using Cu Kα radiation was used to identify crystalline phase of the prepared powders. XRD data were obtained at $2\theta = 10–110^\circ$, with a step size of 0.03° and a count time of 5 s. The collected intensity data of XRD were analyzed by the Rietveld refinement program, *Fullprof* 2002 [23]. Chemical compositions of the resulting powders were analyzed by an atomic absorption spectroscopy (AAS, Analyst 300, Perkin Elmer). For pH measurement, the powders immersed in water were monitored by adding 20 g of the powder to 100 mL purified water (pH 7) with constant stirring with a magnetic stirrer. The pH was measured over a 30–40 min period.

For fabrication of positive electrodes, the prepared powders were mixed with carbon black and polyvinylidene fluoride (90:6:4) in *N*-methylpyrrolidinone. The slurry thus obtained was coated onto Al foil and roll-pressed at 120 °C in air. The electrodes were dried at 120 °C for over-night in vacuum state prior to use. Cell tests were done using R2032 coin-type cell adopting Li metal as the negative electrode. The long cycle-life tests were performed in a laminated type full cell wrapped with Al pouch (thickness, 30 mm; width, 90 mm; and length, 160 mm). Artificial graphite was used as the negative electrode (loading amount: 7 mg cm^{-1} comprising the negative electrode capacity versus the positive electrode capacity of 1.11). The electrolyte solution used was 1 M $LiPF_6$ in ethylene carbonate–dimethyl carbonate (1:2 in volume). A preliminary cell formation was performed for Li-ion cell: five cycles were performed at room temperature at 0.01–0.5 C-rates in the voltage range of 3.0–4.2 V versus graphite.

3. Results and discussions

Fig. 1 shows Rietveld refinement patterns of XRD data for the $Li[Ni_{0.4}Co_{0.2}Mn_{0.4}]O_2$ and the spinel $Li[Li_{0.1}Al_{0.05}Mn_{1.85}]O_4$ compounds. The layer compound (Fig. 1a) presents a well-ordered α-$NaFeO_2$ structure with space group $R\bar{3}m$. Clear peak splittings of (0 0 6)/(1 0 2) and (1 0 8)/(1 1 0) pairs is a good indicative of formation of well-ordered O3 type layer structure. To investigate structural details, Rietveld refinement was performed for the $Li[Ni_{0.4}Co_{0.2}Mn_{0.4}]O_2$. For the refinements, it was supposed that Ni^{2+} located at the 3*b* sites (transition metal layer) can be exchanged with Li^+ occupied at the 3*a* site (lithium layer) due to the similarity of their ionic radii (Li^+: 0.76 Å; Ni^{2+}: 0.69 Å). For Co^{3+} (0.53 Å) and Mn^{4+} (0.54 Å [24]) the ionic radii are much smaller than those of Li^+ so that the possibility of Co^{3+} and Mn^{4+} incorporation into the Li layer is excluded for the refinement. The observed peaks were well matched with the calculated one in Fig. 1a with 10.1% of R_{wp} factor (goodness of fit: 1.67), which represents relatively high reliability. Lattice parameters obtained by the refinement were $a = 2.870(2)$ Å and $c = 14.262(8)$ Å. Site exchange of Ni^{2+} with Li^+ was found to be 3.9% by the refinement.

For the lithium excess spinel $Li[Li_{0.1}Al_{0.05}Mn_{1.85}]O_4$, by assuming that 8*b* and 16*c* sites are vacant, the Rietveld refinement was carried out with the conditions that occupation factor of all elements is invariable and the sum of occupation factor of Mn and Li in 16*d* sites is equal to one. As shown in Fig. 1b, the lithium excess spinel $Li[Li_{0.1}Al_{0.05}Mn_{1.85}]O_4$ has cubic spinel phase, and excess Li and Al are well distributed in 16*d* manganese site with 12.3% of R_{wp} reliable factor (goodness of fit: 2.43). Calculated lattice parameter was 8.215(5) Å. The smaller value is ascribed to the reduced amount of relatively larger Mn^{3+} (0.65 Å [24]) in the structure. Meanwhile, the amount of stable Mn^{4+} (0.54 Å [24]) increases relative to Mn^{3+}.

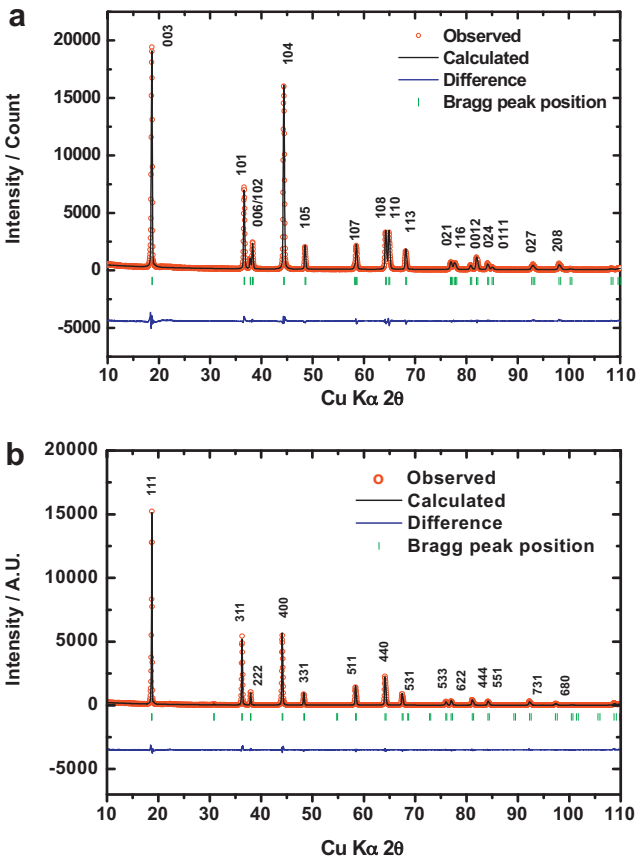

Fig. 1. Rietveld refinement of XRD patterns of (a) as-synthesized $Li[Ni_{0.4}Co_{0.2}Mn_{0.4}]O_2$ and (b) $Li[Li_{0.1}Al_{0.05}Mn_{1.85}]O_4$.

Therefore, the lattice constant is smaller than that of stoichiometric $LiMn_2O_4$ (8.244 Å) [16].

Fig. 2 shows SEM images of the $Li[Ni_{0.4}Co_{0.2}Mn_{0.4}]O_2$ and the spinel $LiMn_2O_4$ compounds. Spherical secondary $Li[Ni_{0.4}Co_{0.2}Mn_{0.4}]O_2$ is composed by submicron primary particles in Fig. 2a. For the spinel $LiMn_2O_4$, it is clear that the compound presents octahedron-shaped particle morphology and the estimated particle size is around 1–2 μm in Fig. 2b. It is expected that such homogeneous distribution of the primary particles can exhibit high power performances.

Fig. 3 presents rate capability of the layer the $Li[Ni_{0.4}Co_{0.2}Mn_{0.4}]O_2$ and the spinel $Li[Li_{0.1}Al_{0.05}Mn_{1.85}]O_4$ measured by coin type half cell that employs Li metal as the negative electrode. Tests were carried out at 25 °C by applying 30 mA g^{-1} (0.2 C-rate) to 1500 mA g^{-1} (10 C-rates) for the $Li[Ni_{0.4}Co_{0.2}Mn_{0.4}]O_2$ in Fig. 3a and 20 mA g^{-1} (0.2 C-rate) to 1000 mA g^{-1} (10 C-rates) for the $Li[Li_{0.1}Al_{0.05}Mn_{1.85}]O_4$ in Fig. 3b. At 0.2 C-rate (30 mA g^{-1}), the $Li[Ni_{0.4}Co_{0.2}Mn_{0.4}]O_2$ delivered a discharge capacity of about 152 mAh g^{-1} with a nominal operation voltage of 3.85 V versus Li in Fig. 3a. With increasing currents, obtained capacities decrease and the operation voltages are as well. At 10 C-rates (1500 mA g^{-1}), it has a discharge capacity of about 90 mAh g^{-1} with a nominal operation voltage of 3.5 V. For the spinel $Li[Li_{0.1}Al_{0.05}Mn_{1.85}]O_4$ compound, we can see that the delivered discharge was around 90 mAh g^{-1} at 0.2 C-rate (20 mA g^{-1}). The capacity was almost maintained at 10 C-rates (1000 mA g^{-1}) with relatively higher nominal operation voltage (3.85 V) in Fig. 3b. When the capacity and operation voltages at 10 C-rates (1000 mA g^{-1}) are compared with those of the layer $Li[Ni_{0.4}Co_{0.2}Mn_{0.4}]O_2$ at 7.5 C-rates (1125 mA g^{-1}), the obtained capacity is obviously much greater of about 30 mAh g^{-1} for the

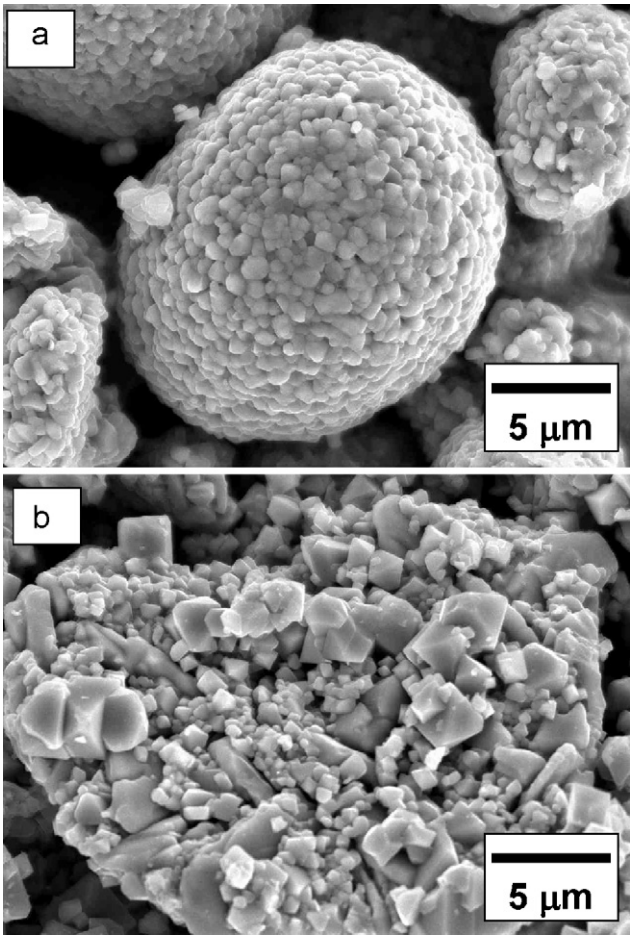

Fig. 2. SEM images of (a) as-synthesized $Li[Ni_{0.4}Co_{0.2}Mn_{0.4}]O_2$ and (b) $Li[Li_{0.1}Al_{0.05}Mn_{1.85}]O_4$.

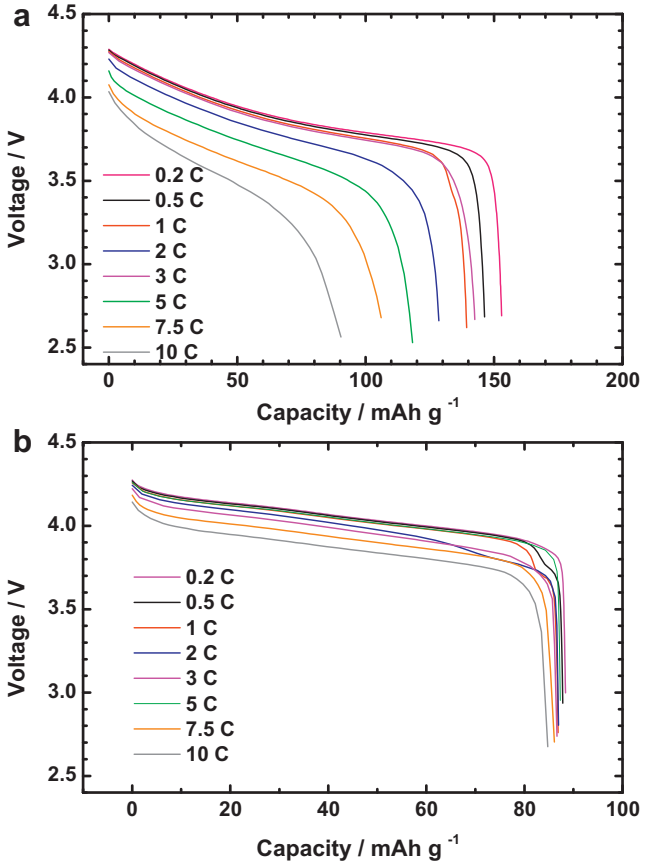

Fig. 3. Rate capability of (a) $Li/Li[Ni_{0.4}Co_{0.2}Mn_{0.4}]O_2$ and (b) $Li/Li[Li_{0.1}Al_{0.05}Mn_{1.85}]O_4$. Tests were carried out at 25 °C by applying 30 mA g^{-1} (0.2 C-rate) to 1500 mA g^{-1} (10 C-rates) for $Li[Ni_{0.4}Co_{0.2}Mn_{0.4}]O_2$ and 20 mA g^{-1} (0.2 C-rate) to 1000 mA g^{-1} (10 C-rates) for $Li[Li_{0.1}Al_{0.05}Mn_{1.85}]O_4$.

layered $Li[Ni_{0.4}Co_{0.2}Mn_{0.4}]O_2$. However, the nominal operation voltage seems to be much higher around 0.25 V for the spinel compound.

Fig. 4 shows rate properties of $C/Li[Ni_{0.4}Co_{0.2}Mn_{0.4}]O_2$ and $C/Li[Li_{0.1}Al_{0.05}Mn_{1.85}]O_4$ cells operated at 25 °C (2.7–4.2 V), respectively. The nominal capacity (at 1 C-rate) was of about 3500 mAh for $C/Li[Ni_{0.4}Co_{0.2}Mn_{0.4}]O_2$ in Fig. 4a and that was close to 3100 mAh for $C/Li[Li_{0.1}Al_{0.05}Mn_{1.85}]O_4$ in Fig. 2. As can be seen in Fig. 4a, the layered $Li[Ni_{0.4}Co_{0.2}Mn_{0.4}]O_2$ which has cation mixing approximately 3.9% presents a gradual decrease in capacity with increasing currents to 10 C-rates. The nominal operation voltage at the current was found to be 3.6 V. Interestingly, though the operation voltage is getting lower, the obtained capacity at 30 C-rates (2870 mAh) is comparable to that at 10 C-rates (2980 mAh). From the variation in the capacity from 1 C to 10 C-rates, it is natural that the cell should have shown the similar rate capability at the higher current that was seen from 1 C to 10 C-rates. It is likely that when the higher currents were applied across the electrodes, the heat induced by the higher currents would be radiated throughout the cell. The increased cell temperature would result in the higher capacity even at 30 C-rates in Fig. 4a. Surprisingly, the spinel compound shows significantly higher capacity retention at 30 C-rates (*ca.* 97%), compared to its discharge capacity at 1 C-rate. The nominal operation voltages were 3.78 V at 10 C-rates and 3.51 V at 30 C-rates in Fig. 4b, which are relatively higher than those observed in Fig. 4a. Those superior rate characteristics of the spinel $Li[Li_{0.1}Al_{0.05}Mn_{1.85}]O_4$ would be due to the intrinsic property of 3-dimensional structured spinel compound, whose Li^+ ion can be de-/intercalated in all directions. The similar tendencies were also observed in the half cell tests of Fig. 3.

The fabricated Li-ion cells were cycled at elevated temperature (60 °C). The cells were charged at 1 C-rate and discharged at 5 C-rates. For the layered $Li[Ni_{0.4}Co_{0.2}Mn_{0.4}]O_2$, one can see in Fig. 5 that the obtained discharge capacity at the current is slightly higher comparing with that of the result at room temperature presented in Fig. 4a. Such phenomenon is usually seen for the layer $Li[Ni_{0.4}Co_{0.2}Mn_{0.4}]O_2$ compound probably due to the improved Li^+ mobility at such elevated operation temperature. Although a slight capacity loss appeared during cycling, the retained capacity after cycling was of about 90% of its initial discharge capacity in Fig. 5. On the other hand the initial discharge capacity for the spinel $Li[Li_{0.1}Al_{0.05}Mn_{1.85}]O_4$ was slightly reduced at 60 °C in Fig. 5 comparing to the capacity at 25 °C (Fig. 4b). This tendency would result from the reaction with HF that is generated by decomposition of electrolytic salt, $LiPF_6$. Since the multiplication of HF is facilitated at elevated temperature, damage of the spinel active material accompanying by the disproportionated dissolution of Mn at the temperature can affect the decrease in the discharge capacity from earlier stage. There is an obvious occurrence of capacity fading during cycling. The capacity retention was relatively poor, but about 65% of its initial capacity was kept during cycling at 5 C-rates. Measured powder pH for the layer $Li[Ni_{0.4}Co_{0.2}Mn_{0.4}]O_2$ was found to be close to 11 so that even though acidic HF is formed as a result of the decomposition of electrolytic salt during cycling, the higher pH would contribute to neutralize the pH of the electrolyte upon cycling. Furthermore, the electrochemically Mn^{4+} in the structure provides tremendous structural stability. For these reasons, the

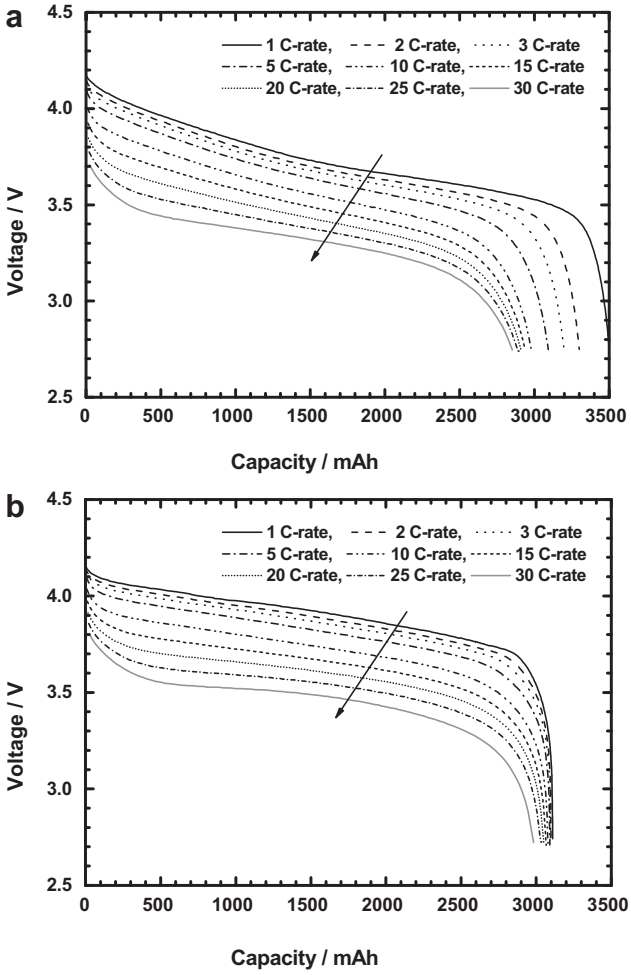

Fig. 4. Rate capability of (a) C/Li[$Ni_{0.4}Co_{0.2}Mn_{0.4}$]O_2 and (b) C/Li[$Li_{0.1}Al_{0.05}Mn_{1.85}$]$O_4$ measured at 25 °C.

higher capacity retention at 60 °C for the layer compound is reasonable. Meanwhile, the measured pH of Li[$Li_{0.1}Al_{0.05}Mn_{1.85}$]$O_4$ was around 9. So, once the active material is exposed to the acid, the active material can be relatively readily acidified by the HF attack during cycling, resulting in serious disproportionated reaction of Mn element. As is well known, Mn^{4+} would reside with active material as electro-inactive Li_2MnO_3 that makes discontinuous network of electron transfer. Mn^{2+} would be deposited on the surface of negative electrode and it is spontaneously reduced to metallic compound. This combination, in turn, deteriorates cell performances with increased cell impedance.

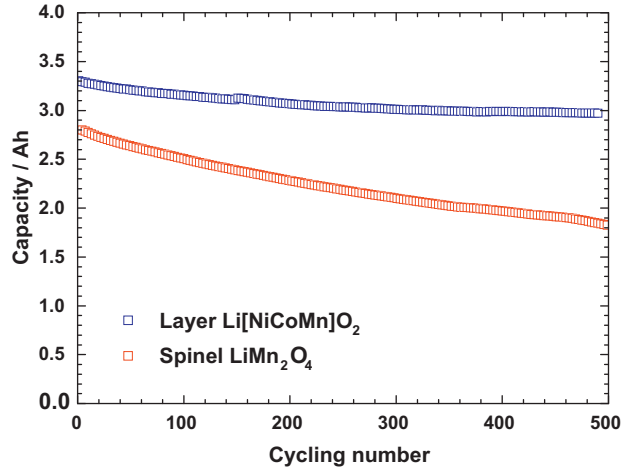

Fig. 5. Cyclability of C/Li[$Ni_{0.4}Co_{0.2}Mn_{0.4}$]O_2 and C/Li[$Li_{0.1}Al_{0.05}Mn_{1.85}$]$O_4$ cell at 60 °C.

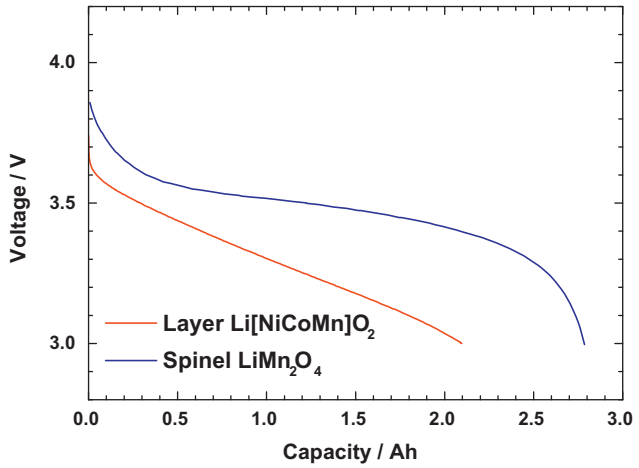

Fig. 6. Low temperature test results of C/Li[$Ni_{0.4}Co_{0.2}Mn_{0.4}$]O_2 and C/Li[$Li_{0.1}Al_{0.05}Mn_{1.85}$]$O_4$ cell measured at −20 °C.

Discharge profiles of the Li[$Ni_{0.4}Co_{0.2}Mn_{0.4}$]O_2 and the spinel Li[$Li_{0.1}Al_{0.05}Mn_{1.85}$]$O_4$ at low temperature (−20 °C) are shown in Fig. 6. After charging by 1 C-rate at 25 °C, the cells were aged for 4 h at the environment and the cells, then, were subsequently discharged at 5 C-rates in the condition. Discharge began at 3.64 V and a linear voltage variation is seen for the layered Li[$Ni_{0.4}Co_{0.2}Mn_{0.4}$]O_2, while the obtained discharge capacity approximated to 2100 mAh in Fig. 6, whose capacity corresponds to 60% of the capacity at 1 C-rate of Fig. 4a. Relatively lower electronic conductivity resulting from the presence of Mn^{4+} and occupation of Ni^{2+} in the layer might be considered as the detrimental factors showing the smaller capacity at low temperature for the layer Li[$Ni_{0.4}Co_{0.2}Mn_{0.4}$]O_2. Spinel compound presented a large discharge capacity at the low temperature in Fig. 6. The delivered capacity was around 2800 mAh, showing a nominal operation voltage at 3.5 V (Fig. 6). Almost 90% of capacity at 1 C-rate of Fig. 4b was retained. The higher capacity retention for the spinel at −20 °C would be related to intrinsic properties of spinel Li[$Li_{0.1}Al_{0.05}Mn_{1.85}$]$O_4$ compound; higher electric conductivity and 3-dimensional Li^+ diffusion from the spinel framework.

4. Conclusions

Layer Li[$Ni_{0.4}Co_{0.2}Mn_{0.4}$]O_2 and spinel Li[$Li_{0.1}Al_{0.05}Mn_{1.85}$]$O_4$ were investigated as positive electrode materials for high power lithium-ion batteries. From Rietveld refinements of XRD data, it was found that the layer Li[$Ni_{0.4}Co_{0.2}Mn_{0.4}$]O_2 presented site exchange between Ni^{2+} and Li^+; 3.9% of Ni^{2+} in the Li layer and the equivalent amount of Li^+ occupied in the transition metal layer. For the spinel Li[$Li_{0.1}Al_{0.05}Mn_{1.85}$]$O_4$, it was found that a small portion of Li was seen in the Mn sites. Both materials consisted of microscale primary particles, but the layer Li[$Ni_{0.4}Co_{0.2}Mn_{0.4}$]O_2 exhibited spherical secondary morphology. They presented superior rate capability at higher currents in 3 Ah lithium-ion cell. The layer Li[$Ni_{0.4}Co_{0.2}Mn_{0.4}$]O_2 had fairly good high temperature properties, but it delivered lower discharge capacity at low temperature. The spinel Li[$Li_{0.1}Al_{0.05}Mn_{1.85}$]$O_4$ showed a gradual capacity at elevated temperature, while it delivered higher discharge capacity at low temperature.

References

[1] K. Amine, J. Liu, ITE Lett. 1 (2000) 59.
[2] R. Kostecki, F. McLarnon, Electrochem. Solid State Lett. 7 (2004) A380.
[3] M.-H. Kim, H.-S. Shin, D. Shin, Y.-K. Sun, J. Power Sources 159 (2006) 1328.
[4] H. Arai, S. Okada, Y. Sakurai, J. Yamaki, Solid State Ionics 109 (1998) 295.
[5] J. Cho, H. Jung, Y. Park, G. Kim, H.S. Lim, J. Electrochem. Soc. 147 (2000) 15.
[6] D.P. Abraham, R.D. Twesten, M. Balasubramanian, I. Petrov, J. McBreen, K. Amine, Electrochem. Commun. 4 (2002) 620.
[7] S.-U. Woo, B.-C. Park, C.S. Yoon, S.-T. Myung, J. Prakash, Y.-K. Sun, J. Electrochem. Soc. 154 (2007) A649.
[8] A.M. Andersson, D.P. Abraham, R. Haasch, S. MacLaren, J. Liu, K. Amine, J. Electrochem. Soc. 149 (2002) A1358.
[9] T. Ohzuku, Y. Makimura, Chem. Lett. (2001) 642.
[10] G.-H. Kim, S.-T. Myung, H.J. Bang, J. Prakash, Y.-K. Sun, Electrochem. Solid-State Lett. 7 (2004) A477.
[11] T Ohzuku, Y. Makimura, Chem. Lett. (2001) 744.
[12] Z. Lu, D.D. MacNeil, J.R. Dahn, Electrochem. Solid-State Lett. 4 (2001) A200.
[13] D.D. MacNeil, Z. Lu, J.R. Dahn, J. Electrochem. Soc. 149 (2002) A1332.
[14] S.-T. Myung, S. Komaba, K. Kurihara, K. Hosoya, N. Kumagai, Y.-K. Sun, I. Nakai, M. Yonemura, T. Kamiyama, Chem. Mater. 18 (2006) 1685.
[15] S. Komaba, N. Kumagai, T. Sasaki, Y. Miki, Electrochemistry 69 (2001) 784.
[16] S.-T. Myung, S. Komaba, N. Kumagai, J. Electrochem. Soc. 148 (2001) A482.
[17] B. Banov, Y. Todorov, A. Trifonova, A. Momchilov, V. Manev, J. Power Sources 68 (1997) 578.
[18] K. Amine, H. Tukamoto, H. Yasuda, Y. Fujita, J. Electrochem. Soc. 143 (1996) 1607.
[19] C. Sigala, A. Vebaere, J.L. Mansot, D. Guyomard, Y. Piffard, T. Tournoux, J. Solid State Chem. 132 (1997) 372.
[20] L. Hernan, J. Morales, L. Sanchez, J. Santos, Solid State Ionics 118 (1999) 179.
[21] M. Hosoya, H. Ikuta, T. Uchida, M. Wakihara, J. Electrochem. Soc. 144 (1997) L52.
[22] M.-H. Lee, Y.-J. Kang, S.-T. Myung, Y.-K. Sun, Electrochim. Acta 50 (2004) 939.
[23] T Roisnel, J. Rodriguez-Carjaval, Fullprof Manual, Institut Laue- Langevin, Grenoble, France, 2002.
[24] R.D. Shannon, Acta Crystallogr. Sect. A: Cryst. Phys. Diffr. Theor. Gen. Crystallogr. 32 (1976) 756.